POLITECNICO DI TORINO
Repository ISTITUZIONALE

Quadratic manifold for model order reduction of a geometrically nonlinear beam with friction contact

Original
Quadratic manifold for model order reduction of a geometrically nonlinear beam with friction contact / Mashayekhi, F., Zucca, S.. - Electromagnetic Problems Arising in Industry: Modelling and Numerical Techniques:(2024). (9th European Congress on Computational Methods in Applied Sciences and Engineering Lisbon (POR) 3–7 June 2024) [10.23967/eccomas.2024.109].

Availability:
This version is available at: 11583/3013492 since: 2026-07-23T23:56:37Z

Publisher:
Scipedia S.L.

Published
DOI:10.23967/eccomas.2024.109

Terms of use:

This article is made available under terms and conditions as specified in the corresponding bibliographic description in the repository

Publisher copyright

(Article begins on next page)

26 November 2026

The 9th European Congress on Computational Methods in Applied Sciences and Engineering
ECCOMAS Congress 2024
3–7 June 2024, Lisboa, Portugal

QUADRATIC MANIFOLD FOR MODEL ORDER REDUCTION OF A GEOMETRICALLY NONLINEAR BEAM WITH FRICTION CONTACT

F. Mashayekhi [1], and S. Zucca[1]

[1] Department of Mechanical and Aerospace Engineering (DIMEAS)
Politecnico di Torino
Corso Duca degli Abruzzi, 24, 10129 Turin, Italy
e-mail: fahimeh.mashaykehi@polito.it

Key words: Nonlinear model order reduction, geometric nonlinearity, friction contact

Summary. This study investigates the application of the quadratic manifold method for model order reduction of geometrically nonlinear structures with friction contact. Quadratic mapping has recently shown its ability to accurately capture the vibrations of a slender structure with geometric nonlinearity. Component Mode Synthesis methods are also well-established reduction approaches for structures with local nonlinearity. These methods allow keeping the contact degrees of freedom (DoFs) in the reduced vector of unknowns and incorporate the corresponding static modes into the reduction basis. In this research, the quadratic manifold method is implemented while contact DoFs are kept in the generalized coordinate vector. So, the manifold is tangent to the subspace spanned by the linear vibration and static modes, and the manifold's curvature is determined by the static derivatives of the linear vibration modes. The inclusion of the static modes enhances the representation of the behavior of a structure under nonlinear friction forces. The proposed reduction approach is evaluated using a simplified model of a cantilever vibrating beam undergoing rubbing against a wall. The reduced model maintains accuracy while reducing the number of the generalized coordinates compared to a linear manifold, resulting in less online computation time. However, the frequent updating of the projection basis at each iteration imposes an extra online computational burden.

1 INTRODUCTION

The relative displacements between the structural components cause friction contacts in many engineering applications like joints [1] and friction dampers [2]. The resulting nonlinear forces contribute significantly to the dynamics of structures. Furthermore, the increasing demand for lighter, more flexible structures is leading to the design of structures more prone to geometric nonlinearity [3]. This increases the likelihood of cases undergoing these two types of nonlinearities simultaneously [4, 5, 6]. For example, aero-engine blades can exhibit both large deformations and rubbing phenomena between the blade and the casing [7]. These nonlinearities lead to complex behavior, while high-fidelity FE models are needed to model these structures accurately. However, the simulation of the dynamic behavior of these structures is very time-consuming. This paper aims to apply model order reduction techniques that allow accurate prediction of the structure behavior within an affordable computational time.

Component Mode Synthesis (CMS) methods [8, 9] are extensively used for the model order reduction of structures with friction contact [10, 11]. These techniques allow for keeping the DoFs subjected to contact forces (contact DoFs) in the reduced vector of unknowns. This

feature removes the requirement for back-and-forth transfer between the reduced and full space in order to have the nonlinear contact forces, and it also makes it possible to compute the nonlinear contact forces accurately. The CMS methods have been enhanced in several studies [12, 13, 15, 14] to capture also the effect of geometric nonlinearity. In these studies, the modal derivatives [16] are added linearly to the CMS basis, which consists of the linear normal modes and a set of static deformations.

The addition of modal derivatives using a quadratic function is proposed in [17, 18] and later studied in [19, 20, 21] for the substructuring of geometrically nonlinear structures. Here, this quadratic mapping method is implemented for the model order reduction of a geometrically nonlinear structure with friction contact such that contact DoFs are kept in the reduced vector of unknowns. The aim is to examine the performance of this reduced model and also to investigate the effect of friction contact on the nonlinear relation between geometrically coupled modes.

This paper is organized as follows: Sec. 2 starts with the reduction of the governing equations. Then, the linear and nonlinear mapping functions and parameters are explained in Secs. 2.1 and 2.2. Finally, the model used to study the reduced model is introduced in the Numerical Analysis Sec. 3 along with the obtained results.

2 METHODOLOGY

The nonlinear dynamics of a structure with elastic material undergoing large displacement/rotation and having frictional contact excited by a periodic external force is governed by the second-order differential equations:

$$\mathbf{M}\ddot{\mathbf{u}}(t) + \mathbf{C}\dot{\mathbf{u}}(t) + \mathbf{f}_{nl}(\mathbf{u}(t)) = \mathbf{f}_e(t) + \mathbf{f}_c(\dot{\mathbf{u}}, \mathbf{u}, t) \tag{1}$$

where $\mathbf{M} \in \mathbb{R}^{N\times N}$ and $\mathbf{C} \in \mathbb{R}^{N\times N}$ represent the mass and viscous damping matrices and $\mathbf{u}(t) \in \mathbb{R}^N$ is the vector of nodal displacement. The force vectors are the internal elastic forces $\mathbf{f}_{nl}(\mathbf{u}(t)) : \mathbb{R}^N \mapsto \mathbb{R}^N$, the time-varying external force vector $\mathbf{f}_e(t) \in \mathbb{R}^N$, and the nonlinear contact forces $\mathbf{f}_c(\dot{\mathbf{u}}, \mathbf{u}, t) : \mathbb{R}^N \mapsto \mathbb{R}^N$. The dots refer to the derivatives with respect to time $t \in \mathbb{R}$.

To keep contact DoFs in the reduced model, first, the vector of displacements is partitioned into two components:

$$\mathbf{u} = \begin{bmatrix} \mathbf{u}_\mathrm{k} \\ \mathbf{u}_\mathrm{p} \end{bmatrix} \tag{2}$$

where $\mathbf{u}_\mathrm{k} \in \mathbb{R}^{N_k}$ is the vector of displacements kept in the newly defined vector of coordinates (generalized coordinates), but $\mathbf{u}_\mathrm{p} \in \mathbb{R}^{N_p}$ is the vector of displacements that will be defined as a function of a small set of modal generalized coordinates $\mathbf{q} \in \mathbb{R}^{n_q}$ and $\mathbf{u}_\mathrm{k}$. So, the generalized coordinate vector $\mathbf{z}(t)$ will be

$$\mathbf{z} = \begin{bmatrix} \mathbf{u}_\mathrm{k} \\ \mathbf{q} \end{bmatrix} \tag{3}$$

A mapping function $\mathbf{\Gamma}(\mathbf{u}, \mathbf{q}) : \mathbb{R}^{n_q+N_k} \mapsto \mathbb{R}^N$ relating the reduced order DoFs $\mathbf{z}$ to the full order DoFs $\mathbf{u}$ is considered as $\mathbf{u} = \mathbf{\Gamma}(\mathbf{u}_\mathrm{k}, \mathbf{q})$ and substituted into governing Eq. 1 to obtain the reduced set of governing equations. According to the principle of virtual work, the residual force is selected to be orthogonal to the tangent projector $\mathbf{P}_\Gamma = \frac{\partial \mathbf{\Gamma}}{\partial \mathbf{z}}$ [18, 22]. Hence, pre-multiplying the resulting equations by the $\mathbf{P}_\Gamma^T$ yields the reduced set of equations:

$$\mathbf{P}_\Gamma^T\mathbf{M}\ddot{\mathbf{\Gamma}} + \mathbf{P}_\Gamma^T\mathbf{C}\dot{\mathbf{\Gamma}} + \mathbf{P}_\Gamma^T\mathbf{f}_{nl}(\mathbf{u}) = \mathbf{P}_\Gamma^T\mathbf{f}_e(t) + \mathbf{P}_\Gamma^T\mathbf{f}_c(\dot{\mathbf{u}}, \mathbf{u}, t) \tag{4}$$

The mapping function $\mathbf{\Gamma}$ form and parameters should be defined to have the reduced equations.

2.1 MAPPING FUNCTION

The parameters of $\mathbf{\Gamma}$ set a reduced basis spanned by a few carefully selected modes. Three sets of modes are assumed here, enabling the simulation of the behavior of a geometrically nonlinear structure with friction contact. The first set consists of the normal modes of the linear system, which are excited by the external forces. The second set includes the structure static deformations referred to as static modes. These modes are considered to describe the contact behavior better and are necessary for keeping physical DoFs in the generalized coordinates. The last set $\mathbf{\Theta}$ includes the modes that are excited due to geometric nonlinearity and are referred to as geometrically coupled modes in this study. To have the function $\mathbf{\Gamma}$, the relation between these modes and physical DoFs should be defined. The linear relation is defined well in literature [24, 25]; however, for the sake of completeness, it is also mentioned here in line with describing the nonlinear relation to better representation of the nonlinear mapping features. The linear and quadratic functions based on free interface CMS reduction techniques are as follows:

$$\mathbf{u}(t) = \mathbf{\Psi}\mathbf{f}_{\mathrm{k}} + \mathbf{\Upsilon} \tag{5}$$

for the linear mapping, the function $\mathbf{\Upsilon}$ is

$$\mathbf{\Upsilon}^{\mathrm{L}} = \mathbf{\Phi}\mathbf{q}_{\phi} + \mathbf{\Theta}^{(2)}\mathbf{q}_{\Theta} \tag{6}$$

while for the quadratic mapping, the function $\mathbf{\Upsilon}$ is

$$\mathbf{\Upsilon}^{\mathrm{NL}} = \mathbf{\Phi}\mathbf{q}_{\phi} + \frac{1}{2}\mathbf{\Theta}^{(3)}\mathbf{q}_{\phi}\mathbf{q}_{\phi} \tag{7}$$

where matrices $\mathbf{\Psi} \in \mathbb{R}^{N\times N_k}$ and $\mathbf{\Phi} \in \mathbb{R}^{N\times n_\phi}$ are, respectively, the residual flexibility attachment modes and free interface normal modes. The geometrically coupled modes in this work are presented by Static Modal Derivatives (SMD) [16], which are gathered in the matrix $\mathbf{\Theta}^{(2)}$ for the linear mapping Eq. 6 and in the third-order tensor $\mathbf{\Theta}^{(3)}$ for the nonlinear mapping Eq. 7. These modes are described more in Sec. 2.2. The modal generalized vectors $\mathbf{q}_\phi \in \mathbb{R}^{n_\phi}$ and $\mathbf{q}_\Theta \in \mathbb{R}^{n_\Theta}$ include the participation factor of normal modes and SMDs, respectively. However, the participation factor of SMDs in nonlinear mapping Eq. 7 is considered a function of the participation factor of the corresponding normal modes. $\mathbf{f}_{\mathrm{k}} \in \mathbb{R}^{N_k}$ is the vector of forces applied to DoFs intended to be kept in the generalized coordinates.

Eq. 5 describes the nodal displacement vector $\mathbf{u}(t)$ as a function of the vector $\mathbf{f}_{\mathrm{k}}$ and the modal generalized coordinates. To replace the force vector $\mathbf{f}_{\mathrm{k}}$ by the nodal displacement vector $\mathbf{u}_{\mathrm{k}}$, Eq. 5 is partitioned into the same components as Eq. 2. Then the force vector $\mathbf{f}_{\mathrm{k}}$ is computed as a function of $\mathbf{u}_{\mathrm{k}}$ from one set of the equations and replaced in the other set resulting in the following equations:

$$\mathbf{u} = \mathbf{\Gamma}(\mathbf{u}_{\mathrm{k}}, \mathbf{q}) = \begin{bmatrix} \mathbf{u}_{\mathrm{k}} \\ \mathbf{\Psi}_{\mathrm{p}}\mathbf{\Psi}_{\mathrm{k}}^{-1}\mathbf{u}_{\mathrm{k}} + \mathbf{\Psi}_{\mathrm{p}}\mathbf{\Psi}_{\mathrm{k}}^{-1}(\mathbf{\Upsilon}_{\mathrm{k}}) + \mathbf{\Upsilon}_{\mathrm{p}} \end{bmatrix} \tag{8}$$

where subscripts p and k refer to the rows of matrices and vectors related to the projected and kept DoFs, respectively. Function $\mathbf{\Gamma}$ stands for the nonlinear mapping $\mathbf{\Gamma}^{\mathrm{NL}}$ if the nonlinear function $\mathbf{\Upsilon}^{\mathrm{NL}}$ is replaced in Eq. 8; otherwise it stands for the linear mapping $\mathbf{\Gamma}^{\mathrm{L}}$.

Now the tangent projector matrix $\mathbf{P}_\Gamma$ could be computed taking into account that the vector of generalized coordinates is $[\mathbf{u}_{\mathrm{k}}^{\mathrm{T}}, \mathbf{q}_\phi^{\mathrm{T}}, \mathbf{q}_\Theta^{\mathrm{T}}]$ for the linear mapping, while it is reduced to $[\mathbf{u}_{\mathrm{k}}^{\mathrm{T}}, \mathbf{q}_\phi^{\mathrm{T}}]$ for the nonlinear mapping. Therefore, the partial derivatives of $\mathbf{\Gamma}$ for the linear mapping will be

$$\mathbf{P}_{\Gamma^{\mathrm{L}}} = \begin{bmatrix} \mathbf{I} & \mathbf{0} & \mathbf{0} \\ \mathbf{\Psi}_{\mathrm{p}}\mathbf{\Psi}_{\mathrm{k}}^{-1} & \mathbf{\Phi}_{\mathrm{p}} + \mathbf{\Psi}_{\mathrm{p}}\mathbf{\Psi}_{\mathrm{k}}^{-1}\mathbf{\Phi}_{\mathrm{k}} & \mathbf{\Theta}_{\mathrm{p}}^{(2)} + \mathbf{\Psi}_{\mathrm{p}}\mathbf{\Psi}_{\mathrm{k}}^{-1}\mathbf{\Theta}_{\mathrm{k}}^{(2)} \end{bmatrix} \tag{9}$$

and for the nonlinear one:

$$\mathbf{P}_{\Gamma^{\text{NL}}} = \begin{bmatrix} \mathbf{I} & \mathbf{0} \\ \boldsymbol{\Psi}_{\text{p}}\boldsymbol{\Psi}_{\text{k}}^{-1} & (\boldsymbol{\Phi}_{\text{p}} + \boldsymbol{\Theta}_{\text{p}}^{(3)}\mathbf{q}_{\phi}) + \boldsymbol{\Psi}_{\text{p}}\boldsymbol{\Psi}_{\text{k}}^{-1}(\boldsymbol{\Phi}_{\text{k}} + \boldsymbol{\Theta}_{\text{k}}^{(3)}\mathbf{q}_{\phi}) \end{bmatrix} \tag{10}$$

These relations show the most important features of the nonlinear mapping that are the state dependency of the tangent projector matrix as well as its smaller size. It is also notable that the participation factors of SMDs are limited to the square of the participation factor of the corresponding normal modes.

The time derivative of the mapping function will be as follows using the chain rule:

$$\dot{\boldsymbol{\Gamma}} = \mathbf{P}_{\Gamma}\dot{\mathbf{z}}, \quad \ddot{\boldsymbol{\Gamma}} = \mathbf{P}_{\Gamma}\ddot{\mathbf{z}} + \frac{\partial \mathbf{P}_{\Gamma}}{\partial \mathbf{z}}\dot{\mathbf{z}}\dot{\mathbf{z}} \tag{11}$$

$$\frac{\partial \mathbf{P}_{\Gamma^{\text{NL}}}}{\partial \mathbf{z}} = \begin{bmatrix} \mathbf{0} & \mathbf{0} \\ \mathbf{0} & \boldsymbol{\Theta}_{\text{p}}^{(3)} + \boldsymbol{\Psi}_{\text{p}}\boldsymbol{\Psi}_{\text{k}}^{-1}\boldsymbol{\Theta}_{\text{k}}^{(3)} \end{bmatrix}, \quad \frac{\partial \mathbf{P}_{\Gamma^{\text{L}}}}{\partial \mathbf{z}} = \mathbf{0}$$

Substituting Eq. 11 and Eq. 10/Eq. 9 in Eq. 4 results in the reduced equation of motion as a function of the generalized coordinates:

$$\bar{\mathbf{M}}\ddot{\mathbf{z}} + \mathbf{P}_{\Gamma}^{T}\mathbf{M}\frac{\partial \mathbf{P}_{\Gamma}}{\partial \mathbf{z}}\dot{\mathbf{z}}\dot{\mathbf{z}} + \bar{\mathbf{C}}\dot{\mathbf{z}} + \bar{\mathbf{f}}_{nl}(\mathbf{u}) = \bar{\mathbf{f}}_{e}(t) + \bar{\mathbf{f}}_{c}(\dot{\mathbf{u}}, \mathbf{u}, t) \tag{12}$$

where the reduced mass matrix $\bar{\mathbf{M}} \in \mathbb{R}^{n\times n}$, reduced damping matrix $\bar{\mathbf{C}} \in \mathbb{R}^{n\times n}$, and reduced forces vector $\bar{\mathbf{f}}_{e/c/nl}(t) \in \mathbb{R}^{n}$ are given by

$$\bar{\mathbf{M}} = \mathbf{P}_{\Gamma}^{T}\mathbf{M}\mathbf{P}_{\Gamma}, \quad \bar{\mathbf{C}} = \mathbf{P}_{\Gamma}^{T}\mathbf{C}\mathbf{P}_{\Gamma}, \quad \bar{\mathbf{f}}_{e/c/nl}(t) = \mathbf{P}_{\Gamma}^{T}\mathbf{f}_{e/c/nl}(t). \tag{13}$$

The convective term $\mathbf{P}_{\Gamma}^{T}\mathbf{M}\frac{\partial \mathbf{P}_{\Gamma}}{\partial \mathbf{z}}\dot{\mathbf{z}}\dot{\mathbf{z}}$ is additional compared to full order equation of motion Eq. 1 which appears in nonlinear mapping. Eq. 12 is numerically integrated with the implicit Newmark method (average acceleration method) [26] to reach steady state response. In each time step, this second-order nonlinear equation is solved by the Newton/-Raphson algorithm.

2.2 MAPPING BASIS

Rubin reduction technique as a free interface CMS method relies on the normal and static modes of the structure with open contact in which the contact surfaces are fully separate. The projection basis of this technique consists of free interface normal modes, residual flexibility attachment matrix, and rigid body modes. Since the vibration behavior of structures that are not free–free individually is under investigation, rigid body modes are not included here.

The structure deformation due to a unit force applied at a kept DoF is an attachment mode. These modes correspond to the columns of the flexibility matrix $\mathbf{G}$ related to the kept DoFs $\mathbf{G}^{\text{k}}$. Removing the contribution of the retained free interface normal modes from the set of attachment modes matrix $\mathbf{G}^{\text{k}}$ results in the residual flexibility attachment matrix $\boldsymbol{\Psi}$:

$$\boldsymbol{\Psi} = \mathbf{G}^{\text{k}} - \sum_{p=1}^{n_{\phi}} \frac{\boldsymbol{\phi}_p \boldsymbol{\phi}_p^{T}}{\omega_p^2} \tag{14}$$

where ω_p is the natural frequency of pth free interface normal mode $\boldsymbol{\phi}_p$.

Modal derivatives are obtained by taking the derivative of the generalized eigenvalue problem of the linearized system around an arbitrary displacement state such that the internal elastic

forces are cast in the form $\mathbf{f}_{\text{int}} = \mathbf{K}\mathbf{u}$. Ignoring the inertia term, the so-called *S*tatic Modal Derivatives (SMDs) are computed while they can also be derived by the differentiation of the nonlinear static equation [24, 25]. Hence, the static derivative of the i_{th} normal mode with respect to the amplitude of the j_{th} normal mode, $\boldsymbol{\theta}_{ij}$, is as follow:

$$\boldsymbol{\theta}_{ij} = \frac{\partial \boldsymbol{\phi}_i}{\partial q_j} = -\mathbf{K}^{-1}\mathbf{K}'_j\boldsymbol{\phi}_i \tag{15}$$

where $\mathbf{K}'_j$ is the derivative of the tangent stiffness matrix ($\mathbf{K}$) with respect to a displacement in the direction of $\boldsymbol{\phi}_j$. It is prominently approximated nonintrusively via finite differences. The central finite difference yields the following formulation [18]:

$$\mathbf{K}'_j = \frac{\partial \mathbf{K}}{\partial q_j}\Big|_{\text{eq}} = \frac{\mathbf{K}(\mathbf{u} = \boldsymbol{\phi}_j h) - \mathbf{K}(\mathbf{u} = -\boldsymbol{\phi}_j h)}{2h} \tag{16}$$

The SMDs do not feature orthogonality to linear modes, so a Gram–Schmidt process is employed to provide a linearly independent basis. The size of a complete set of SMDs that can be computed from n modes is quadratic to n. However, due to their symmetry, $N_{\text{d}} = n_\phi(n_\phi{+}1)/2$ unique SMDs can be computed. Therefore, the SMD matrix ($\boldsymbol{\Theta}^{(2)}$) for the linear mapping takes the form:

$$\boldsymbol{\Theta}^{(\mathbf{2})} = [\boldsymbol{\theta}_{11}, \boldsymbol{\theta}_{12}, ..., \boldsymbol{\theta}_{1n_\phi}, \boldsymbol{\theta}_{22}, ..., \boldsymbol{\theta}_{n_\phi n_\phi}] \tag{17}$$

However, the tensor of SMDs ($\boldsymbol{\Theta}^{(3)}$) in the nonlinear mapping function Eq. 7 is consisted of n_ϕ matrix while i_{th} matrix $\boldsymbol{\Theta}_i^{(3)}$ include the derivatives of i_{th} mode with respect to others such that:

$$\boldsymbol{\Theta}_i^{(3)} = [\boldsymbol{\theta}_{\text{i1}}, \boldsymbol{\theta}_{\text{i2}}, ..., \boldsymbol{\theta}_{\text{i}n_\phi}] \tag{18}$$

The number of SMDs grows quadratically with the number of linear modes. So, it is important to find the most relevant SMDs, particularly for the linear mapping that the size of the equation increases by the number of SMDs. To achieve this the Maximum Modal Interaction (MMI) criterion proposed by Tiso [23] is used which requires a linear run under external loading over time [0,T], then the weighting of each SMD is computed:

$$W_{ij} = \max|\eta_i(t)|.\max|\eta_j(t)| \tag{19}$$

where $\eta_i(t)$ is the time-varying amplitude of the ith mode. The SMDs that have the greatest W_{ij} value will be chosen.

2.3 REDUCED NONLINEAR FORCES

The intrusive method is used to compute the reduced nonlinear forces in Eq. 12 which means that the full-order nonlinear forces are computed as a function of the physical displacements. It requires the mapping of the generalized coordinates to the physical displacements (Eq. 8) and also the mapping of the full-order nonlinear forces to the reduced space (Eq. 13). In other words, a back-and-forth exchange between the ROM and the FEM variables is needed at each iteration of the numerical solver as shown in Figure. 1.

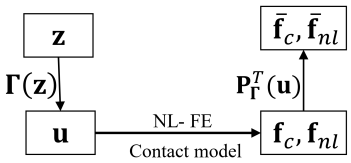

Figure 1: Computation of internal elastic forces and contact forces

The difference between linear and nonlinear mapping in the procedure shown in Figure. 1 is that the mapping function is constant in linear one but it is state-dependent in nonlinear one and should be computed in each iteration. It is also noteworthy that if a non-intrusive method is used to compute the internal elastic forces, there will be no need to transfer between full and reduced space because the reduced force will be computed directly as a function of the generalized coordinate. These methods are not the topic of this study.

Nonlinear elastic forces $\mathbf{f}_{\mathrm{nl}}$ arise from large displacements and rotations, leading to a nonlinear relation between displacement and strain, while the material behavior remains within the linear elastic range. The Nonlinear Finite Element method (NL-FE) is employed to compute the nonlinear elastic forces. However, the nonlinear contact forces $\mathbf{f}_{\mathrm{c}}$ are due to the relative displacement between two components, and a contact element [27, 28] is used to compute them. The contact model is shown in Figure. 2, the contact parameters are the tangential and normal contact stiffness k_t and k_n, respectively, and a friction coefficient between the contact surfaces μ. The relative displacements in the tangential and normal directions are $u(t)$ and $v(t)$, respectively, while the amount of tangential slip between the contact surfaces is $w(t)$.

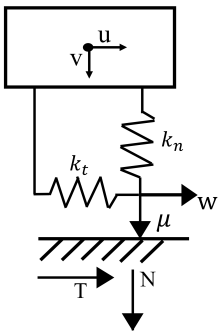

Figure 2: Contact model with 1D tangential displacement and variable normal load

During oscillation, the contact state alternates between slip, stick, and liftoff. Normal contact force (N) and tangential contact force (T) are defined as:

$$\mathrm{N} = \max(N_0 + k_n \mathrm{v}, 0) \quad ; \quad \mathrm{T} = \begin{cases} k_t(\mathrm{u} - \mathrm{w}) & \text{stick state} \\ \mathrm{sgn}(\dot{\mathrm{w}})\mu \mathrm{N} & \text{slip state} \\ 0 & \text{lift-off state} \end{cases} \tag{20}$$

where N_0 is the static normal load obtained based on a preliminary static analysis. The normal and tangential contact forces are added to $\mathbf{f}_{\mathrm{c}}$ vector considering the required coordinate transformation. In terms of contact states, two limit cases could be regarded as full-liftoff and full-stick configurations in which contact is, respectively, in liftoff and stick states at all time steps during a period of oscillation. The structure characteristics in full-liftoff configuration are

similar to the structure without contact while in full-stick configuration the structure behaves like one with added contact stiffness. The Frequency Response Functions (FRF) of the model considered in this study are presented in different contact configurations in the presence of geometric nonlinearity.

3 NUMERICAL ANALYSIS

The dynamic response of a geometrically nonlinear cantilever beam under periodic excitation is examined to investigate the performance of the previously discussed techniques. A friction contact is considered at the beam tip as seen in Fig. 3. The beam motion is described in plane $(\mathbf{e}_x, \mathbf{e}_y)$ which are the axial and transverse coordinates, respectively. Axis $\mathbf{e}_x$ is along the beam neutral axis in undeformed configuration while $\mathbf{e}_y$ is perpendicular to it. Notably, this model can be assumed as a simplified representation of the rubbing interaction between the blade and casing in gas turbines with an assumed rigid casing and disk.

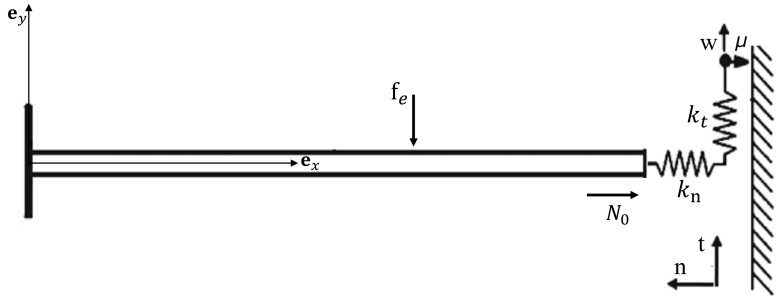

Figure 3: Model of a planar cantilever beam with friction contact at its end.

The beam length is L = 2.54 m and internal structural damping is introduced as mass-proportional viscous damping, where $\alpha = 5$. The beam material properties are Young's modulus $E = 207$ GPa, density $\rho = 7801$ kg/m^3, and Poisson's ratio of $\nu = 0.28$. The beam cross-section is square with area $A = 0.6451$ m^2. A harmonic force with the amplitude of $F_e = 111.29$ N in a constant direction (y coordinate) is applied on the beam. A FE beam model based on a total Lagrangian nonlinear formulation and a Timoshenko kinematics [29] is considered. This model consists of 20 elements while each node has 3 DoFs.

The contact state is dependent on the static normal load N_0 and contact parameters, including contact stiffness and the friction coefficient. The effects of these parameters have been studied extensively in the literature [30]. Here, the friction coefficient and contact stiffness are considered as $\mu = 0.5$ and $k_t = k_n = 10$ N/mm.

To provide a better understanding of the dynamics of the structure under study, initially, the forced response analysis of its full order model is studied. The frequency response functions of the beam at four values of the static normal preload ($N_0 = 0, 40, 80$, and 350 N) are shown in Figure 4. In the case of blade–casing rubbing interaction, the normal preload N_0 is due to the centrifugal force acting on a rotating blade. The reference system is the so-called open contact ($N_0 = 0$ N) corresponding to the cantilever beam with no friction contact.

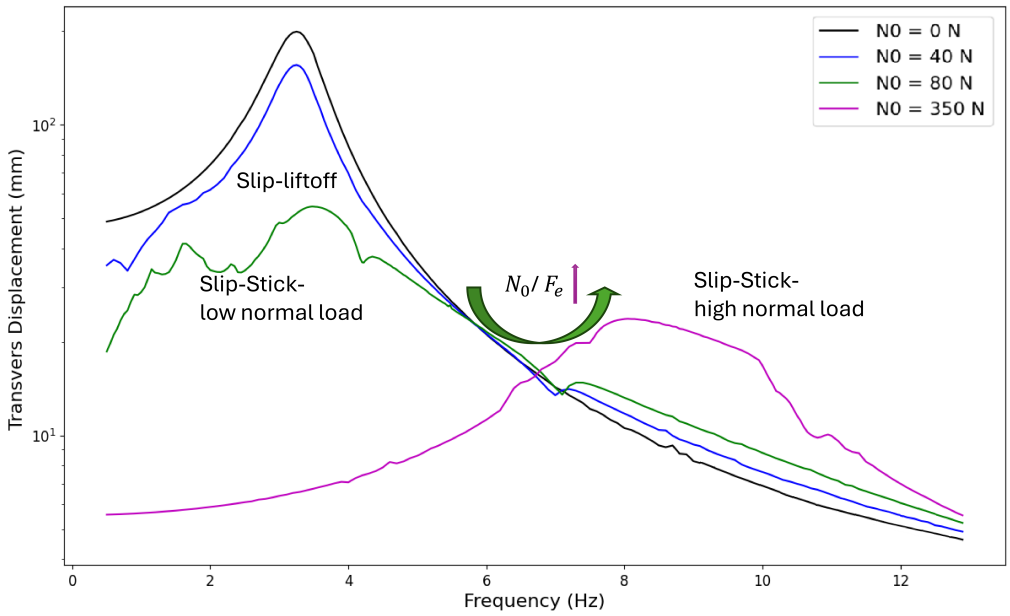

Figure 4: Frequency response function of the beam tip with four values of contact normal preload.

Figure 4 shows that in agreement with literature [30], when normal preload increases, there is an initial fall in resonance amplitude because of the increased energy dissipation ($N_0 = 40$ and 80 N). However, when normal preload grows, there is an increase in resonance amplitude and frequency ($N_0 = 350$ N) because of the higher stiffening effect of the contact.

The goal of this study is to investigate the quadratic relation between geometrically coupled modes in different contact conditions and to evaluate the performance of the quadratic manifold method for the forced response analysis of the geometrically nonlinear structures with friction contact. In order to do this, three resonance points with different contact configurations are considered which occur at the specific normal loads and excitation frequencies: a) $N_0 = 40$ N, $Freq = 3.2$ Hz, b) $N_0 = 80$ N, $Freq = 3.5$ Hz, and c) $N_0 = 350$ N, $Freq = 8.2$ Hz.

The hysteresis loop, the contact tangential force vs. tangential displacement in a period of oscillation, is shown in Figure. 5 at the aforementioned contact configurations. Based on the contact states that the structure undergoes, the contact configurations are called Slip-Liftoff ($N_0 = 40$ N, $Freq = 3.2$ Hz), Slip-Stick low normal load ($N_0 = 80$ N, $Freq = 3.5$ Hz), and Slip-Stick high normal load ($N_0 = 350$ N, $Freq = 8.2$ Hz). The beam tip contact node in Slip-Liftoff configuration undergoes slip and liftoff states. As a result, the amplitude of vibration is 21 % smaller than the maximum amplitude of the reference system (open contact) due to the energy dissipated by friction during slip. However, the resonance frequency is the same as the reference system. The contact alternate slip and stick in higher normal loads while the slip state is dominated in Slip-Stick low normal load configuration, although, the stick state dominates in slip-stick high normal load configuration.

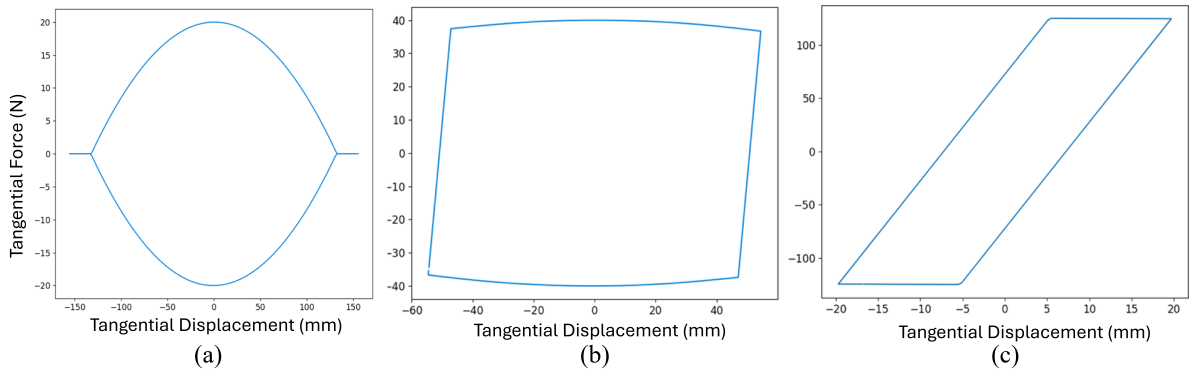

Figure 5: Hysteresis loop in (a) Slip-Liftoff, (b) Slip-Stick low normal load, and (c) Slip-Stick high normal load

In these three configurations, the relation between geometrically coupled modes is investigated using linear mapping in which the contribution factors of the SMDs ($\mathbf{q}_\Theta$) are also unknown. Then, the accuracy and efficiency of the quadratic mapping method are examined.

3.1 QUADRATIC MANIFOLD

Quadratic relation between geometrically coupled modes which are here the axial and transverse modes is examined by the application of the linear mapping. So, first, the linear Rubin reduced model is built with the 1st vibration mode ϕ_1, 2 residual flexibility attachment modes, and the first modal derivative of the 1st vibration mode θ_{11}. Then the steady-state response of the beam is obtained using this model in Slip-Liftoff configuration. In Figure. 6, the SMD's contribution factor $q_{\theta_{11}}$ and the half of the square of the first vibration mode's contribution factor (${q_{\phi_1}}^2/2$) are plotted in a period of vibration versus the 1st vibration mode's contribution factor q_{ϕ_1} and its time derivative $\dot{q}_{\phi_1}$.

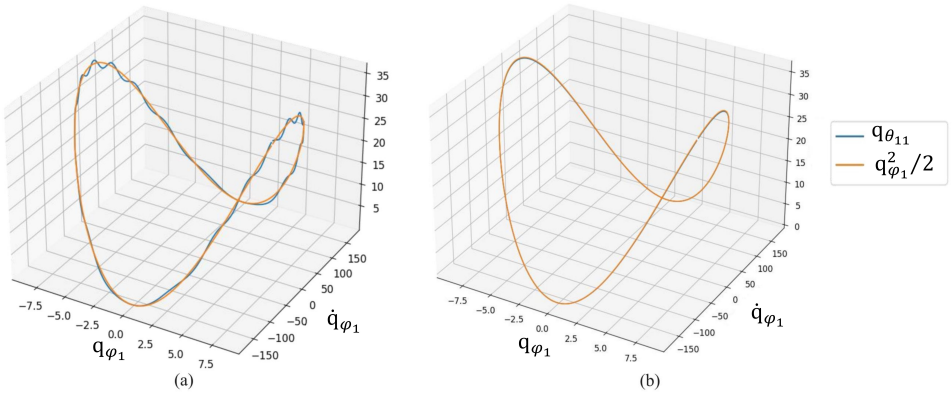

Figure 6: Modes contribution factor (a) without and (b) with orthogonalization of modal derivatives with respect to static modes

Figure. 6 (a) shows the results when the static modal derivative is not orthogonalized to the residual flexibility attachment modes. In this case, the error in the computed amplitude of the beam tip is 3.55 %. After orthogonalization, this error diminishes to 1.87 % while there is also a perfect match between contribution factor plots which admit the quadratic relation

between the axial and transverse modes in this contact state and load level. The analysis is performed with the Linear Rubin ROM of the same size in the slip-stick contact configurations. The same results are obtained in terms of the quadratic relation between the contribution factor of transverse and axial modes. However, the percentage error is not the same. In Table. 3.1, the errors of the beam tip amplitude obtained by the linear and quadratic manifolds and their computational time difference are shown:

Table 1: Beam tip amplitude error using linear and quadratic mapping and the percentage of difference between the computational time in different contact configurations

Contact configuration	Rubin Linear	Rubin Quadratic	Time difference %
Slip liftoff	1.87 %	2.79 %	+0.008%
Slip-Stick low normal load	2.75 %	2.37 %	-0.005%
Slip stick-high normal load	11.2 %	11.1 %	+0.22%

The results presented in this table show that in slip-stick contact configuration with a high normal preload, the error is noticeably larger. Taking into consideration the low amplitude of vibration in this contact configuration, it could not be due to geometric nonlinearity. Indeed, the nonlinear contact stiffness added to the system is higher and the first free interface normal mode is not enough to simulate the structure displacement. So the second vibration mode is added to the basis. The error of the linear and quadratic Rubin with the size of five and four, respectively, will be reduced to 2.36 % and 1.36 %.

In Figure. 7, the participation factors of the 2nd normal mode $\boldsymbol{\phi}_2$ and 1st SMD $\boldsymbol{\theta}_{11}$ ($q_{\theta_{11}}$ and q_{ϕ_2}) and the half of the square of participation of $\boldsymbol{\phi}_1$ ($q_{\phi_1}^2/2$) are plotted against q_{ϕ_1} in Slip-Stick high normal load contact configuration.

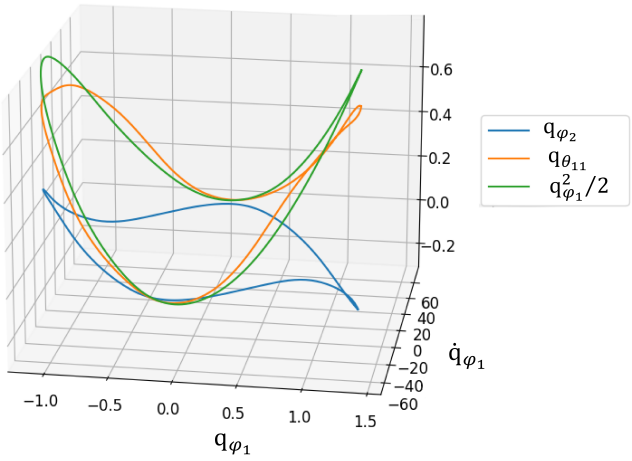

Figure 7: Modal contribution factor of the modal derivatives and second vibration mode vs. Modal contribution factor of the first vibration mode

Figure. 7 shows that the quadratic relation $q_{\theta_{11}} = q_{\phi_1}^2/2$ is no longer valid in this configuration. However, since the amplitude of vibration is very low, this approximation still yields an acceptable accuracy (Error = 1.36 %). This figure also depicts the nonlinear relation between

the contribution factors of the 1st and 2nd linear normal modes (q_{ϕ_1} and q_{ϕ_2}) which is due to the nonlinear effects of contact [31].

The other considerable point in Table. 3.1 is the computational time difference between the two methods. It is expected that due to the smaller size of the nonlinear reduced model, the computational time will be less with nonlinear mapping. However, the time is only smaller in the Slip-Stick low normal load contact configuration. This is due to two reasons: first, the computation of the projection matrix in each solution iteration; more importantly, it is due to the higher number of iterations needed to reach convergence via nonlinear mapping.

4 CONCLUSIONS

In this article, the Rubin method is enhanced to capture the behavior of a geometrically nonlinear structure with friction contact by the addition of the Static Modal Derivatives using a quadratic function. It shows that the contact DoFs could be kept in the generalized coordinate while a nonlinear relation is defined between the generalized and physical DoFs.

The methodology is applied to a cantilever beam model with friction contact at its tip. Three contact configurations with different contact states are investigated using the linear function, where the contribution factors of the geometrically coupled modes are unknown. It has been shown that the nonlinear relation between geometrically coupled modes holds in the presence of friction forces only in Slip-liftoff and Slip-Stick low preload. It is also important that the static modes added to keep contact DoFs are orthogonal to Static Modal Derivatives. As expected, the accuracy of quadratic mapping was comparable to linear mapping; however, the computational time is not always reduced.

The next steps will be using non-intrusive methods to compute the internal elastic forces considering the effect of contact configuration on structure dynamics.

FUNDING

This research is supported by the Horizon Europe framework program under the Marie Skłodowska-Curie Actions grant agreement 101061195.

REFERENCES

[1] Brake, M. R. (2016). The mechanics of jointed structures. Cham: Springer.

[2] Fantetti, A., Setchfield, R., & Schwingshackl, C. (2023). Nonlinear dynamics of turbine bladed disk with friction dampers: Experiment and simulation. International Journal of Mechanical Sciences, 257, 108510.

[3] Capiez-Lernout, E., Soize, C., & Mbaye, M. (2014, September). Geometric nonlinear dynamic analysis of uncertain structures with cyclic symmetry-Application to a mistuned industrial bladed disk. In International Conference on Uncertainty in Structural Dynamics, USD2014 (pp. 1-14).

[4] Alcorta, R., Chouvion, B., Michon, G., & Montagnier, O. (2023). On the use of frictional dampers for flutter mitigation of a highly flexible wing. International Journal of Non-Linear Mechanics, 156, 104515.

[5] Delhez, E., Nyssen, F., Golinval, J. C., & Batailly, A. (2021). Assessment of geometric nonlinearities influence on NASA rotor 37 response to blade tip/casing rubbing events. Journal of Engineering for Gas Turbines and Power, 143(11), 111022.

[6] Dattaguru, B., Everett Jr, R. A., Whitcomb, J. D., & Johnson, W. S. (1984). Geometrically nonlinear analysis of adhesively bonded joints.

[7] Piollet, E., Nyssen, F., & Batailly, A. (2019). Blade/casing rubbing interactions in aircraft engines: Numerical benchmark and design guidelines based on NASA rotor 37. Journal of Sound and Vibration, 460, 114878.

[8] Craig Jr, R. R., & Bampton, M. C. (1968). Coupling of substructures for dynamic analyses. AIAA journal, 6(7), 1313-1319.

[9] Rubin, S. (1975). Improved component-mode representation for structural dynamic analysis. AIAA journal, 13(8), 995-1006.

[10] Charleux, D., Gibert, C., Thouverez, F., & Dupeux, J. (2006). Numerical and experimental study of friction damping blade attachments of rotating bladed disks. International Journal of Rotating Machinery, 2006(1), 071302.

[11] Petrov, E. P., & Ewins, D. J. (2006). Effects of damping and varying contact area at blade-disk joints in forced response analysis of bladed disk assemblies.

[12] Balmaseda, M., Jacquet-Richardet, G., Placzek, A., & Tran, D. M. (2020). Reduced order models for nonlinear dynamic analysis with application to a fan blade. Journal of Engineering for Gas Turbines and Power, 142(4), 041002.

[13] Delhez, E., Nyssen, F., Golinval, J. C., & Batailly, A. (2020, September). Comparative study of blades reduced order models with geometrical nonlinearities and contact interfaces. In Turbo Expo: Power for Land, Sea, and Air (Vol. 84232, p. V011T30A017). American Society of Mechanical Engineers.

[14] Shetty, D., Allen, M., & Park, K. (2023). A new approach to model a system with both friction and geometric nonlinearity. Journal of Sound and Vibration, 552, 117631.

[15] Delhez, E., Nyssen, F., Golinval, J. C., & Batailly, A. (2023). Numerical study of bladed structures with geometric and contact nonlinearities. Journal of Sound and Vibration, 544, 117382.

[16] Idelsohn, S. R., & Cardona, A. (1985). A reduction method for nonlinear structural dynamic analysis. Computer Methods in Applied Mechanics and Engineering, 49(3), 253-279.

[17] Jain, S., Tiso, P., Rutzmoser, J. B.,& Rixen, D. J. (2017). A quadratic manifold for model order reduction of nonlinear structural dynamics. Computers & Structures, 188, 80-94.

[18] Rutzmoser, J. B., Rixen, D. J., Tiso, P., & Jain, S. (2017). Generalization of quadratic manifolds for reduced order modeling of nonlinear structural dynamics. *Computers & Structures*, 192, 196-209.

[19] Gomes de Camargos Silveira, L., & Hartvig Hansen, M. (2023).Modal Veering Effect on Quadratic Manifold Model Order Reduction Accuracy.

[20] Seawright, J. (2023). Non-Intrusive Nonlinear Reduced-Order Model Identification and Substructuring of Geometrically Nonlinear Structures (Doctoral dissertation, University of Washington).

[21] Tian, W. (2023). Substructuring methods for responses, response sensitivity, and model updating of nonlinear systems.

[22] Nicolaidou, E., Hill, T. L., & Neild, S. A. (2022). Nonlinear mapping of non-conservative forces for reduced-order modelling. *Proceedings of the Royal Society A*, 478(2268), 20220522.

[23] Tiso, P. (2011, February). Optimal second order reduction basis selection for nonlinear transient analysis. In Modal Analysis Topics, Volume 3: Proceedings of the 29th IMAC, A Conference on Structural Dynamics, 2011 (pp. 27-39). New York, NY: Springer New York.

[24] Wu, L., Tiso, P.,& Van Keulen, F. (2016, September). A modal derivatives enhanced Craig-Bampton method for geometrically nonlinear structural dynamics. In Proceedings of the 27th International Conference on Noise and Vibration Engineering (pp. 3615-3624).

[25] Wu, L., Tiso, P., Tatsis, K., Chatzi, E., & van Keulen, F. (2019). A modal derivatives enhanced Rubin substructuring method for geometrically nonlinear multibody systems. Multibody system dynamics, 45, 57-85.

[26] Gastaldi, C., & Berruti, T. M. (2018). Competitive time marching solution methods for systems with friction-induced nonlinearities. Applied Sciences, 8(2), 291.

[27] Yang, B. D., Chu, M. L., & Menq, C. H. (1998). Stick–slip–separation analysis and non-linear stiffness and damping characterization of friction contacts having variable normal load. Journal of Sound and vibration, 210(4), 461-481.

[28] Sanliturk, K. Y., & Ewins, D. J. (1996). Modelling two-dimensional friction contact and its application using harmonic balance method. Journal of sound and vibration, 193(2), 511-523.

[29] Felippa, C. A., Crivelli, L. A., & Haugen, B. (1994). A survey of the core-congruential formulation for geometrically nonlinear TL finite elements. Archives of computational methods in engineering, 1, 1-48.

[30] Firrone, C. M., & Zucca, S. (2011). Modelling friction contacts in structural dynamics and its application to turbine bladed disks. Numerical Analysis-Theory and Application, 14, 301-334.

[31] Laxalde, D.,& Thouverez, F. (2009). Complex non-linear modal analysis for mechanical systems: application to turbomachinery bladings with friction interfaces. Journal of sound and vibration, 322(4-5), 1009-1025.